Structural Optimization of Silica-Based 2 × 2 Multimode Interference Coupler Using a Real-Coded Micro-Genetic Algorithm

Takashi Yasui*, Jun-ichiro Sugisaka, and Koichi Hirayama

Abstract—We propose a structural optimization method based on a real-coded micro-genetic algorithm to realize a weakly guided 2 × 2 multimode interference (MMI) coupler with low imbalance and excess loss over a wavelength range from 1520 to 1580 nm. The proposed method was applied to silica-based 2 × 2 MMI couplers with a relative refractive index difference of 5.5%. The optimized result showed an imbalance of less than 8.4×10^{-3} dB, an excess loss of less than 0.14 dB, and a normalized output power of more than 48% over the operation wavelength range. The proposed method achieved an optimized 2 × 2 MMI coupler after 250 times of propagation analysis per wavelength, which is less than 6.7% of those by the conventional methods for 4 × 4 and 1 × 4 MMI couplers, and was proven to be more effective than the conventional methods. To consider realistic optical devices, 2 × 2 MMI couplers whose values of structural parameters are close to the optimized values within the accuracy of typical fabrication tolerance are also analyzed. The results are comparable to those of the optimized 2 × 2 MMI coupler.

1. INTRODUCTION

A multimode interference (MMI) coupler is an important and widely used component in photonic integrated circuits (PICs), such as 3-dB couplers [1–3], optical hybrids [4–6], multi/demultiplexers for mode-division multiplexing (MDM) transmission [7, 8], Mach-Zehnder interferometers for wavelength meters [9], and differential phase shift keying (DPSK) demodulators [10]. An MMI coupler with M input and N output access waveguides is referred to as an $M \times N$ MMI coupler. The most widely used application of a MMI coupler is possibly the 2 × 2 MMI coupler as a 3-dB coupler [1–5].

To fabricate PICs, the most promising and widely used materials are Si nano wire [1, 7, 8, 10], InP [2, 3, 6, 9], and silica [4, 5, 11]. All these materials have drawbacks and advantages. The InP and Si nano wire waveguides are advantageous for high-density integration and integration of active elements such as photo-detectors, but have drawbacks such as high propagation loss and high coupling loss to single-mode fibers (SMFs). On the other hand, the silica waveguides have advantages such as extremely low propagation loss, low coupling loss to SMFs, and low polarization dependence, but the silica waveguides are larger than those of the InP or Si nano wires. To overcome this disadvantage, silica waveguides with high refractive index difference between core and clad have been used to realize compact silica waveguides, as reported recently [11].

In general, the structural parameters of an MMI coupler, such as its length and the positions of the input and output access waveguides, are determined by the self-imaging theory [12], which relies on a parabolic distribution of effective indices of eigenmodes in the MMI section. However, an MMI coupler designed by the self-imaging theory cannot give good performance, such as imbalanced output power and higher excess loss, for an MMI based on a weakly guided waveguide, such as a silica waveguide.

This is because the distribution of effective indices of eigenmodes in the weakly guided MMI section is sub parabolic owing to the larger effective width of higher-order eigenmodes.

To realize a higher-performance weakly-guided MMI coupler, structural optimizations of MMI couplers by the wavefront matching (WFM) method [13] and genetic algorithms (GAs) [14, 15] have been considered. Sugiyama and Tsuda have carried out structural optimization of silica-based 2×2 MMI couplers for the T- and O-bands by the WFM method [13]. Wang et al. [14] and West and Honkanen [15] have applied GAs to structural optimizations of weakly guided 4×4 and 1×4 MMI couplers, respectively, that were operated in a single wavelength.

The WFM method synthesizes the optimized refractive index distribution of the waveguides from the desired optical characteristics [16]. However, very fine refractive index patterns appear in the synthesized optimum waveguides. As a result, the high fabrication tolerance of MMI couplers owing to their simple structure becomes diminished.

The GA optimizes the structural parameters of the MMI couplers, such as the length of the MMI and positions of the access waveguides [14, 15]. Thus, the simple structure of an MMI coupler can be kept through the optimization. In the simplest form of a GA (SGA) [17], an MMI coupler is represented as a binary coded chromosome, and the typical size of the population in a generation is from 30 to 200. However, the binary chromosome representation meets difficulties to optimize the parameters represented by the continuous numbers, such as the structural parameters for an MMI coupler. In addition, since wave propagation analysis is required for the structural optimization of MMI couplers, large population sizes increase the computational time. To overcome such drawbacks of the SGA, a real-coded GA [18], in which the chromosome is represented by a vector of floating point numbers, and a micro-GA (µGA) [19–23], in which the population size is typically five, have been proposed.

In this paper, we propose a method for structural optimization of 2×2 MMI couplers based on a real-coded µGA. The two-dimensional beam-propagation method (BPM) based on the finite-element scheme (FE-BPM) [24–26], whose accuracy for optical waveguide analysis has been ensured [25, 27], is employed for the propagation analysis of the MMI couplers. The proposed method is applied to the optimization of silica-based 2×2 MMI couplers to realize an MMI with low imbalance and low excess loss over a range of operation wavelength from 1520 to 1580 nm. An MMI coupler optimized by the proposed method has an imbalance of less than 8.4×10^{-3} dB, an excess loss of less than 0.14 dB, and a normalized output power of more than 48% over the range of operation wavelength, which are better than the values of an MMI coupler optimized by the WFM method [13]. In addition, the proposed method has an advantage in computational efficiency, because it required less than 6.7% of number of propagation analysis for the optimization, compared to the conventional GA [14, 15].

2. REAL-CODED MICRO-GENETIC ALGORITHM

2.1. Micro-Genetic Algorithm

A µGA is a genetic algorithm with a small population, which is typically five, and reinitialization. It starts with a randomly generated population. Production of individuals in the next generation by genetic operation is carried out until nominal convergence is reached. Then, a new population is generated by transferring the best individual in the converged population to the new one, followed by randomly generating the remaining individuals [19, 20].

The procedures of the algorithm are the following:

(i) Randomly generate the starting population of size $N_p = 5$.

(ii) Perform BPM [24–26] calculations for each individual in the population.

(iii) Evaluate the fitness of each individual in the population.

(iv) The individual with the highest fitness is carried to the next generation as the elite (elitist strategy).

(v) If nominal convergence is reached, randomly generate the remaining $N_p - 1$ individuals in the next generation; otherwise produce the remaining $N_p - 1$ individuals by selection and crossover.

(vi) Repeat (ii)–(v) until the termination condition is satisfied.

2.2. Real-Coded Genetic Algorithm

In the real-coded GA, a chromosome is represented as a vector of floating point numbers [18]. The size of the chromosome is the same as the length of the vector. Each gene, which is represented as an element of the vector, denotes a variable to be optimized.

In this paper, we denote the chromosome of the ith individual in the gth generation as

$$\boldsymbol{x}^{(g,i)} = (x_1^{(g,i)}, x_2^{(g,i)}, \ldots, x_N^{(g,i)}), \tag{1}$$

where N is the size of the chromosome.

To generate the starting population or the remaining $N_p - 1$ individuals after nominal convergence, the value of $x_j^{(g,i)}$ is randomly chosen from an interval $[x_{j,\min}, x_{j,\max}]$, which is the search range of the jth gene.

To produce the $N_p - 1$ individuals in the next generation from individuals in the current generation, a binary tournament selection and the BLX-α strategy [18] are applied to the selection and crossover, respectively.

The selection mechanism produces an intermediate population of size N_p. The elite is copied into the intermediate population. The remaining $N_p - 1$ individuals in the intermediate population are selected by binary tournament selection. The fitness values of two randomly selected individuals in the current generation are compared, and then the individual with the higher fitness is selected for the intermediate population.

The crossover operation produces an individual in the next generation from two randomly selected individuals in the intermediate population. In the BLX-α crossover strategy, the jth gene in the ith individual in the next generation is produced as

$$x_j^{(g+1,i)} = \begin{cases} x_{j,\min} & \text{for } x_j' < x_{j,\min} \\ x_{j,\max} & \text{for } x_j' > x_{j,\max} \\ x_j' & \text{otherwise,} \end{cases} \tag{2}$$

where x_j' is a randomly chosen number of an interval $[x_{j1} - \alpha \cdot I_j, x_{j2} + \alpha \cdot I_j]$ and α is a real number to determine the interval. Here, $x_{j1} = \min(x_j^{g,i_1}, x_j^{g,i_2})$, $x_{j2} = \max(x_j^{g,i_1}, x_j^{g,i_2})$, $I_j = x_{j2} - x_{j1}$, where i_1 and i_2 denote the indices of the randomly selected individuals.

3. MODEL OF 2×2 MMI COUPLER

Figure 1 shows a two-dimensional model of the 2×2 MMI coupler, which has a width and length of W_{MMI} and L_{MMI}, respectively. Two pairs of input and output access waveguides of width w_{ac} are symmetrically placed about the center of the MMI section. The distance between a center of the access waveguide and the center of the MMI is denoted as y_{ac}. The refractive indices of the core and cladding are n_{core} and n_{clad}, respectively.

In this paper, y_{ac} and L_{MMI} are given as follows:

$$L_{MMI} = \frac{3L_\pi}{2} + \Delta L_{MMI}, \tag{3}$$

$$y_{ac} = \frac{W_{MMI}}{4} + \Delta y_{ac}, \tag{4}$$

where ΔL_{MMI} and Δy_{ac} are, respectively, deviations of the length of the MMI and the position of the center of the access waveguides. Here, L_π is the beat length in the MMI given by

$$L_\pi = \frac{\pi}{\beta_0 - \beta_1}, \tag{5}$$

where β_0 and β_1 respectively denote the propagation constants of the fundamental and first-order modes of the MMI. We note that L_{MMI} with $\Delta L_{MMI} = 0$ is the length of a 2×2 MMI coupler given by the self-imaging theory [12].
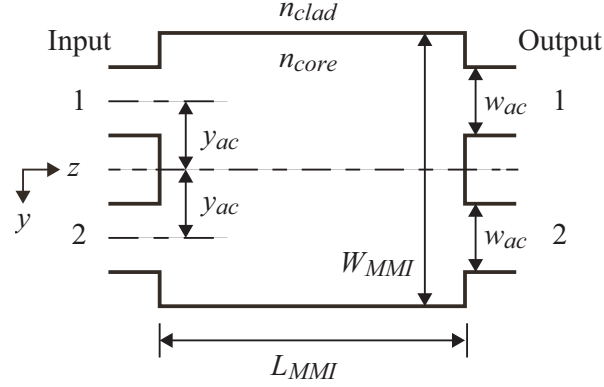
Figure 1. Schematic structure of the 2×2 MMI coupler.

Table 1. Genes and their search ranges for the 2×2 MMI coupler.

j	$x_j^{(g,i)}$	$x_{j,\min}$	$x_{j,\max}$
1	W_{MMI}	$8\,\mu m$	$18\,\mu m$
2	ΔL_{MMI}	$-10\,\mu m$	$10\,\mu m$
3	Δy_{ac}	$-1\,\mu m$	$1\,\mu m$

In the proposed structural-optimization method for 2×2 MMI couplers, the optimum values of W_{MMI}, ΔL_{MMI}, and Δy_{ac} are searched by the real-coded μGA described above. The genes in a chromosome, which represents a 2×2 MMI coupler, and their search ranges are shown in Table 1.

The fitness of each individual is evaluated as follows:

$$F = \exp\left[-\frac{1}{N_\lambda} \sum_{\lambda \in \Lambda} \left(W_{ib} I_b(\lambda) + W_{xl} X_l(\lambda) \right) \right], \tag{6}$$

where Λ is a set of wavelengths for BPM analysis, N_λ denotes the number of elements that belong to Λ, $I_b(\lambda)$ and $X_l(\lambda)$ are the imbalance and excess loss at a wavelength $\lambda \in \Lambda$, respectively, and W_{ib} and W_{xl} are the weighting coefficients that determine the relative importance of $I_b(\lambda)$ and $X_l(\lambda)$, respectively. Here, $I_b(\lambda)$ and $X_l(\lambda)$ are defined as follows:

$$I_b(\lambda) = -10 \log \frac{\min\{P_1(\lambda), P_2(\lambda)\}}{\max\{P_1(\lambda), P_2(\lambda)\}} \text{ [dB]}, \tag{7}$$

$$X_l(\lambda) = -10 \log \frac{P_1(\lambda) + P_2(\lambda)}{P_{in}(\lambda)} \text{ [dB]}, \tag{8}$$

where $P_i(\lambda)$ $(i = 1, 2)$ denotes the output optical power at the output i for the incident wave of power $P_{in}(\lambda)$ into the input 1. We note that $P_i(\lambda)$ $(i = 1, 2)$ are evaluated by the overlap integral at the end of the MMI section, and that the electric field in the BPM calculation is normalized so that $P_{in}(\lambda)$ is unity.

4. NUMERICAL RESULTS

We consider silica-based 2×2 MMI couplers. The range of operation wavelength is from 1520 to 1580 nm. The relative refractive index difference is $\Delta = 5.5\%$ [11]. The wavelength-dependent refractive index of the cladding is given by the following Sellmeier equation [28],

$$n_{clad}(\lambda) = \sqrt{1 + \sum_{i=1}^{3} \frac{a_i \lambda^2}{(\lambda^2 - b_i)}}, \tag{9}$$

where λ is the wavelength in µm, $a_1 = 0.6965325$, $a_2 = 0.4083099$, $a_3 = 0.8968766$, $b_1 = 4.368309 \times 10^{-3}$, $b_2 = 1.394999 \times 10^{-2}$, and $b_3 = 9.793399 \times 10^1$. The widths of the input and output waveguides are taken as $w_{ac} = 3.0$ µm. The thickness of the core is assumed to be 3.0 µm. Two-dimensional models obtained by the effective index method are analyzed by the BPM. The incident wave is assumed to be the TE-polarized fundamental mode of the input access waveguide 1. The termination condition of the optimization process is given as $g = N_i$, where N_i denotes the number of iterations. In the following results, N_i is taken as 50, α for the BLX-α is taken as 0.5, and the propagation constants β_0 and β_1 in Eq. (5) are evaluated at the wavelength of 1550 nm to determine the length of the MMI couplers.

First, to take into account the wavelength dependence of the 2×2 MMI coupler in the optimization process, we consider the three sets of wavelength Λ as $\Lambda_1 = \{1550\,\text{nm}\}$, $\Lambda_3 = \{\lambda_i | \lambda_i = 1520 + 30i\,\text{nm}, i = 0, 1, 2\}$, and $\Lambda_7 = \{\lambda_i | \lambda_i = 1520 + 10i\,\text{nm}, i = 0, 1, 2, \ldots, 6\}$. For each Λ, the optimization process was carried out 100 times. Fig. 2 shows the wavelength dependence of the normalized output power of the optimized structure with the largest fitness after 100 optimization processes for each Λ. Here, the weighting coefficients are taken as $W_{ib} = W_{xl} = 1$. Fig. 2(a) shows the results with $\Lambda = \Lambda_1$ and Λ_3. For $\Lambda = \Lambda_1$, although, very large normalized output power of 49.6% is achieved at the wavelength of 1550 nm, which is used for the optimization, the wavelength dependence of the output power is also very large. On the other hand, the result with $\Lambda = \Lambda_3$ shows the output power of more than 48.5% over the range of operation wavelength with small wavelength dependence. We can see that optimization with more than one wavelength is effective to design a wideband 2×2 MMI coupler. Fig. 2(b) shows the results with $\Lambda = \Lambda_3$ and Λ_7. They show similar output power and wavelength dependence. The obtained structural parameters and the fitness of the optimized 2×2 MMI couplers are shown in Table 2. Since a larger number of wavelengths for the BPM analysis requires longer computational time, we choose Λ_3 as Λ in the following optimization.
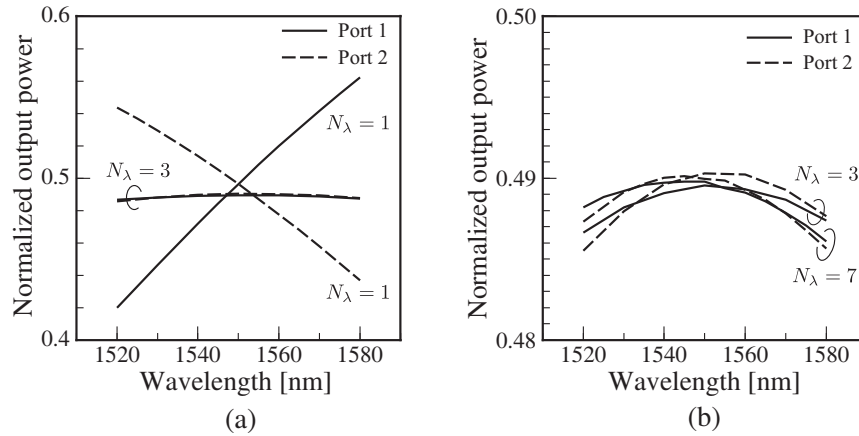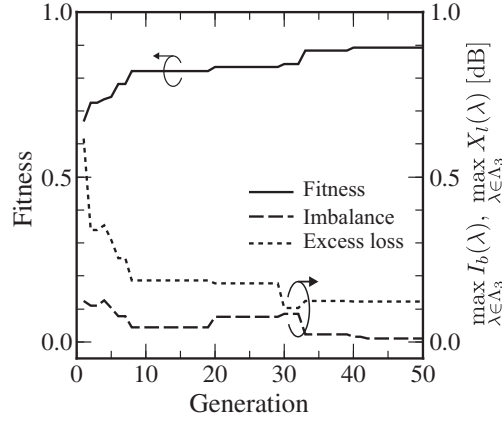

Figure 2. Normalized output power of the optimized 2×2 MMI couplers, which have the highest fitness after 100 optimization processes with (a) $\Lambda = \Lambda_1$ and Λ_3, and (b) $\Lambda = \Lambda_3$ and Λ_7, as functions of wavelength. Here, the incident power at the wavelength λ, $P_{in}(\lambda)$, is normalized to unity.

Table 2. Structural parameters and fitness for the optimized 2×2 MMI couplers with the optimization with $\Lambda = \Lambda_1$, Λ_3, and Λ_7.

Λ	W_{MMI} [µm]	L_{MMI} [µm]	y_{ac} [µm]	fitness
Λ_1	9.466	218	1.520	0.967
Λ_3	8.823	192	2.895	0.892
Λ_7	8.792	191	2.865	0.902

Figure 3 shows the maximum fitness, maximum imbalance, and maximum excess loss as functions of generation for the 2×2 MMI coupler whose normalized output power is shown in Fig. 2 for $\Lambda = \Lambda_3$. We can see that the performance of the 2×2 MMI coupler is improved by the iteration of the optimization

Figure 3. Fitness, maximum imbalance, and maximum excess loss of the optimized 2×2 MMI coupler, which has the highest fitness after 100 optimization processes with $\Lambda = \Lambda_3$, as functions of generation in optimization process.
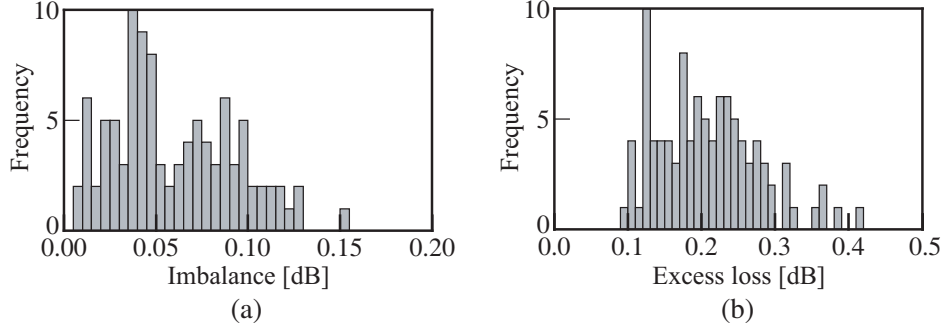

Figure 4. Histograms of maximum (a) imbalance and (b) excess loss for the optimized 2×2 MMI couplers for 100 optimization processes with Λ_3.

process. For the optimized structure, the imbalance and excess loss are smaller than 1.0×10^{-2} dB and 0.12 dB, respectively, over the range of the wavelength of operation. Fig. 4 shows the histograms of the maximum imbalance and excess loss for the 100 optimized structures with $\Lambda = \Lambda_3$. The mean and standard deviation of the imbalance are $\mu_{ib} = 0.060$ dB and $\sigma_{ib} = 0.033$ dB, respectively, and those for the excess loss are $\mu_{xl} = 0.208$ dB and $\sigma_{xl} = 0.069$ dB, respectively. The three standard deviations above the mean for the imbalance and excess loss are, respectively, 0.16 dB and 0.41 dB, which are comparable to the maximum imbalance and excess loss of a weakly guided 2×2 MMI coupler whose structure was optimized by the WFM method [13]. We can say that the proposed optimization method almost always leads to weakly guided 2×2 MMI couplers, which have imbalance values and excess loss values that are as good as or better than those for the WFM method.

The optimum design of MMI couplers requires a large number of optical wave propagation analyses. In the conventional optimization methods based on the conventional GA, propagation analyses were carried out 12000 $[N_p = 80, N_i = 150, N_p \times N_i = 12000]$ times and 3750 $[N_p = 15, N_i = 250, N_p \times N_i = 3750]$ times per wavelength for the optimizations of 4×4 [14] and 1×4 [15] MMI couplers, respectively. In comparison to the conventional method, propagation analyses were carried out 250 $[N_p = 5, N_i = 50, N_p \times N_i = 250]$ times, which is less than 6.7% of those by the conventional methods, per wavelength in the proposed method. The effectiveness of the proposed method is demonstrated through the above examples.

Next, we provide the weighting value W_{xl} as $1 - W_{ib}$ for $0 \le W_{ib} \le 1.0$ to see the effect of the weighting values. The maximum imbalance and excess loss as functions of W_{ib} are shown in Fig. 5. It is evident that the maximum imbalance and excess loss are nearly independent of the value of W_{ib}
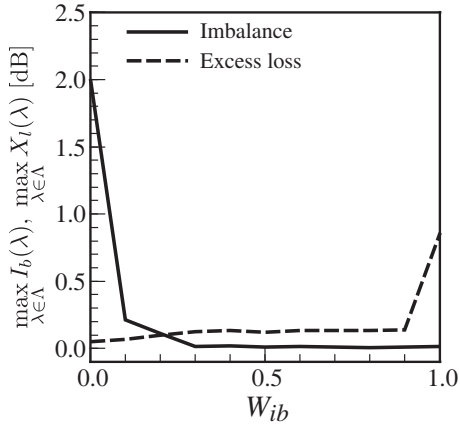
Figure 5. Maximum imbalance and excess loss of the optimized 2×2 MMI couplers as functions of the weighting value W_{ib}. Here, the weighting value W_{xl} is given as $1 - W_{ib}$.
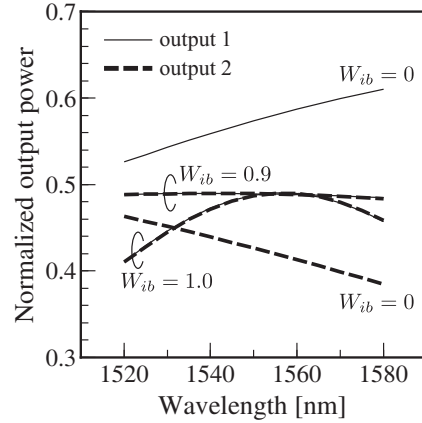

Figure 6. Normalized output power of the optimized 2×2 MMI couplers as a function of wavelength for W_{ib} = 0, 0.9, and 1.0. We note that the output power at output 1 and 2 are identical for W_{ib} = 0.9 and 1.0 owing to small imbalance. Here, the incident power at the wavelength of λ, $P_{in}(\lambda)$, is normalized be unity.

between 0.3 and 0.9. On the other hand, the maximum imbalance and excess loss are very large for $W_{ib} = 0$ [$W_{xl} = 1$] and $W_{ib} = 1$ [$W_{xl} = 0$], respectively. The structural parameters and fitness of the optimized 2×2 MMI couplers are shown in Table 3. Similar structural parameters were achieved for W_{ib} between 0.3 and 0.9. We can say that both the imbalance and excess loss should be considered in the fitness to realize a 2×2 MMI coupler with smaller imbalance and excess loss.

Table 3. Structural parameters and fitness for the optimized 2×2 MMI couplers for the values of W_{ib} between 0 and 1. Here, $W_{xl} = 1 - W_{ib}$ and $\Lambda = \Lambda_3$.

| W_{ib}	$W_{MMI}\,[\mu\mathrm{m}]$	$L_{MMI}\,[\mu\mathrm{m}]$	$y_{ac}\,[\mu\mathrm{m}]$	fitness
0.0	8.217	173	1.649	0.977
0.1	8.149	167	2.554	0.932
0.2	9.878	234	3.392	0.925
0.3	8.834	192	2.896	0.926
0.4	8.830	192	2.901	0.934
0.5	8.854	192	2.865	0.945
0.6	8.735	190	2.854	0.953
0.7	8.866	192	2.848	0.965
0.8	8.798	191	2.855	0.975
0.9	8.836	191	2.831	0.985
1.0	14.970	503	4.413	0.993

Figure 6 shows the normalized output power of the optimized 2×2 MMI couplers as a function of wavelength for W_{ib} = 0, 0.9, and 1.0. We note that W_{ib} = 0.9 gave the largest fitness of the optimized 2×2 MMI coupler for $0.3 \leq W_{ib} \leq 0.9$, as shown in Table 3, where the maximum imbalance and excess loss are less than 8.4×10^{-3} dB and 0.14 dB, respectively. For W_{ib} = 0.9, a normalized output power of more than 48% over the range of operation wavelength was achieved. On the other hand, the normalized output powers of the two output waveguides are not balanced and strongly depend on wavelength for
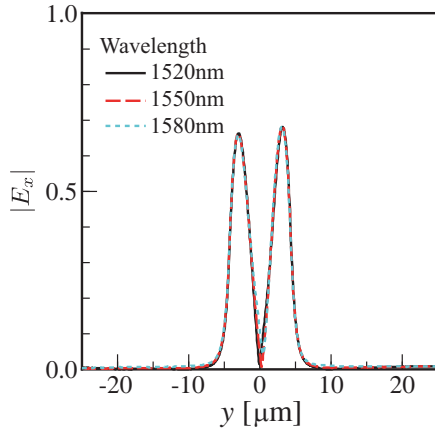
Figure 7. Field distributions at the end of the optimized 2×2 MMI coupler with $W_{ib} = 0.9$. Here, the field is normalized by the amplitude of the incident field.
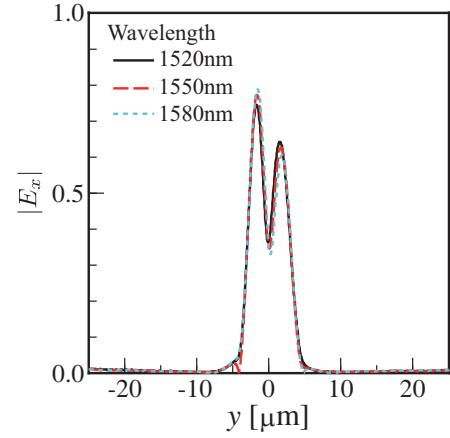
Figure 8. Field distributions at the end of the optimized 2×2 MMI coupler with $W_{ib} = 0$. Here, the field is normalized by the amplitude of the incident field.
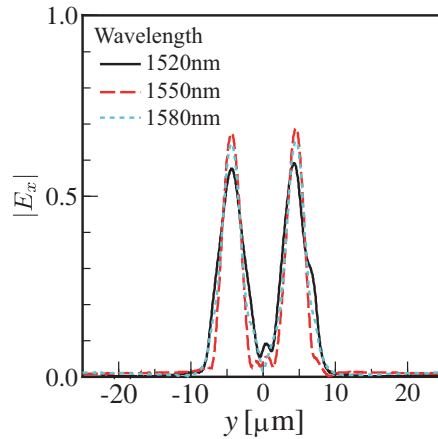
Figure 9. Field distributions at the end of the optimized 2×2 MMI coupler with $W_{ib} = 1.0$. Here, the field is normalized by the amplitude of the incident field.

$W_{ib} = 0$, and they are balanced but the values decrease for longer and shorter wavelengths for $W_{ib} = 1.0$. Distributions of the x-components of the electric field at the end of the optimized 2×2 MMI couplers are shown in Figs. 7, 8, and 9 for $W_{ib} = 0.9$, 0, and 1.0 respectively. As shown in Fig. 7, the input wave is almost equally split without wavelength dependence of the field distribution. On the other hand, Fig. 8 shows non-uniform splitting of the input wave. In Fig. 9, although the input waves are equally split, the peak intensities strongly depend on wavelength.

Since the optimized structural parameters of MMI couplers are represented as floating point values in the chromosome, these values have more precise accuracy than typical fabrication tolerances, which are of the order of $0.1\,\mu$m. We evaluate MMI couplers whose values of W_{MMI} and y_{ac} are around the optimized values for $W_{ib} = 0.9$ with accuracy of typical fabrication tolerance. Table 4 shows the maximum excess loss and imbalance over the operation wavelength range for the MMI couplers with values of W_{MMI} and y_{ac} with the accuracy of fabrication tolerance, where L_{MMI} is taken as $191\,\mu$m. The maximum excess loss of the MMI coupler with $8.8\,\mu$m of W_{MMI} and $2.8\,\mu$m of y_{ac} is identical to that for the optimized structure. Although the maximum imbalance of this MMI coupler is slightly larger than that of the optimized structure, the value is still very small. A normalized output power of more than 48% is achieved. The maximum excess loss and imbalance shown in Table 4 are debased by considering the fabrication tolerance for W_{MMI} and y_{ac}, and are rather sensitive to the change in

Table 4. Maximum excess loss and imbalance over the operation wavelength range for 2×2 MMI couplers whose values of W_{MMI} and y_{ac} are around the optimized values with the accuracy of typical fabrication tolerance. Here, L_{MMI} is taken as 191 μm.

W_{MMI} [μm]	y_{ac} [μm]	max. excess loss [dB]	max. imbalance [dB]
8.8	2.8	0.18	1.1×10^{-1}
8.8	2.9	0.14	2.9×10^{-2}
8.9	2.8	0.33	2.6×10^{-1}
8.9	2.9	0.20	6.7×10^{-1}

W_{MMI}. The authors think that the difference in propagation distance in the MMI section affects the quality of self-imaging characteristics.

5. CONCLUSION

In this paper, we propose a structural optimization method based on a real-coded μGA for weakly guided 2×2 MMI couplers to realize an MMI coupler with low imbalance and excess loss over the wavelength ranging from 1520 to 1580 nm. The proposed method was applied to silica-based 2×2 MMI couplers with $\Delta = 5.5\%$. The optimized 2×2 MMI coupler, which has the MMI section width and length of 8.836 μm and 191 μm, respectively, and for witch the distance between the centers of the MMI and an access waveguide was 2.831 μm, showed an imbalance of less than 8.4×10^{-3} dB, an excess loss of less than 0.14 dB, and a normalized output power of more than 48% over the wavelength range. The proposed method achieved an optimized 2×2 MMI coupler after 250 times of propagation analyses per wavelength, which is less than 6.7% of those by the conventional methods for 4×4 and 1×4 MMI couplers, and was proven to be more effective than the conventional methods. The 2×2 MMI couplers, which have structural parameter values close to the optimized values, within an accuracy of typical fabrication tolerance, were also analyzed by the BPM. The result was comparable with that for the optimized 2×2 MMI coupler.

REFERENCES

1. Chen, S., X. Fu, J. Wang, Y. Shi, S. He, and D. Dai, "Compact dense wavelength-division (de)multiplexer utilizing a bidirectional arrayed-waveguide grating integrated with a Mach-Zehnder interferometer," *J. Lightwave Technol.*, Vol. 33, No. 11, 2279–2285, June 2015.

2. Bitincka, E., G. Gilardi, and M. K. Smit, "On-wafer optical loss measurements using ring resonators with integrated sources and detectors," *IEEE Photon. J.*, Vol. 6, No. 5, 6601212, Oct. 2014.

3. Ma, Y., S. Park, L. Wang, and S. T. Ho, "Ultracompact multimode interference 3-dB coupler with strong lateral confinement by deep dry etching," *IEEE. Photon. Technol. Lett.*, Vol. 12, No. 5, 492–494, May 2000.

4. Sakamaki, Y., Y. Nasu, T. Hashimoto, K. Hattori, T. Saida, and H. Takahashi, "Reduction of phase-difference deviation in 90° optical hybrid over wide wavelength range," *Ieice Electronics Express*, Vol. 7, No. 3, 216–221, Feb. 2010.

5. Hashizume, Y., T. Goh, Y. Inoue, K. Hamamoto, and M. Itoh, "Polarization beam splitter with different core widths and its application to dual-polarization optical hybrid," *J. Lightwave Technol.*, Vol. 33, No. 2, 408–414, Jan. 2015.

6. Fandiño, J. S. and P. Muñoz, "Manufacturing tolerance analysis of an MMI-based 90° optical hybrid for InP integrated coherent receivers," *IEEE Photon. J.*, Vol. 5, No. 2, Apr. 2013.

7. Uematsu, T., Y. Ishizaka, Y. Kawaguchi, K. Saitoh, and M. Koshiba, "Design of a compact two-mode multi/demultiplexer consisting of multimode interference waveguides and a wavelength-insensitive phase shifter for mode-division multiplexing transmission," *J. Lightwave Technol.*, Vol. 30, No. 15, 2421–2426, Aug. 2012.

8. Han, L., S. Liang, H. Zhu, C. Zhang, and W. Wang, "A high extinction ratio polarization beam splitter with MMI couplers on InP substrate," *IEEE Photon. Technol. Lett.*, Vol. 27, No. 7, 782–785, Apr. 2015.

9. Kleijn, E., E. M. van Vliet, D. Pustakhod,, M. K. Smit, and X. J. M. Leijtens, "Amplitude and phase error correction algorithm for 3×3 MMI based Mach-Zehnder interferometers," *J. Lightwave Technol.*, Vol. 33, No. 11, 2233–2239, Jun. 2015.

10. Hai, M. S., M. N. Sakib, and O. Liboiron-Ladouceur, "Monolithic 1×2 MMI-based 25-Gb/s SOI DPSK demodulator integrated with SiGe photodetector," *IEEE Photon. Technol. Lett.*, Vol. 27, No. 6, 565–568, Mar. 2015.

11. Takahashi, M., Y. Uchida, S. Yamasaki, J. Hasegawa, and T. Yagi, "Compact and low-Loss coherent mixer based on high Δ ZrO$_2$-SiO$_2$ PLC," *J. Lightwave Technol.*, Vol. 32, No. 17, 3081–3088, Sept. 2014.

12. Soldano, L. B. and E. C. M. Pennings, "Optical multi-mode interference devices based on self-imaging: Principles and applications," *J. Lightwave Technol.*, Vol. 13, No. 4, 615–627, Apr. 1995.

13. Sugiyama, K. and H. Tsuda, "Broadband 2×2 multimode interference coupler for T- and O-band communication by wavefront matching method," *Advanced Photon.*, JM3A.32, 2015.

14. Wang, Q., J. Lu, and S. He, "Optimal design of a multimode interference coupler using a genetic algorithm," *Opt. Commu.*, Vol. 209, 131–136, Aug. 2002.

15. West, B. R. and S. Honkanen, "MMI devices with weak guiding designed in three dimensions using a genetic algorithm," *Opt. Express*, Vol. 12, No. 12, 2716–2722, Jun. 2004.

16. Sakamaki, Y., T. Saida, T. Shibata, Y. Hida, T. Hashimoto, M. Tamura, and H. Takahashi, "Y-branch waveguides with stabilized splitting ratio designed by wavefront matching method," *IEEE Photon. Technol. Lett.*, Vol. 18, No. 7, 817–819, Apr. 2006.

17. Goldberg, D. E., *Genetic Algorithms in Search, Optimization and Machine Learning*, Addison-Wesley, Boston, USA, 1989.

18. Herrera, F., M. Lozano, and J. L. Verdegay, "Tackling real-coded genetic algorithms: Operators and tools for behavioural analysis," *Artificial Intelligence Review*, Vol. 12, No. 4, 265–319, Aug. 1998.

19. Krishnakumar, K., "Micro-genetic algorithms for stationary and nonstationary function optimization," *SPIE: Intelligent Control and Adaptive Systems*, Vol. 1196, 289–296, Feb. 1989.

20. Coello, C. A. C. and G. T. Pulido, "A micro-genetic algorithm for multiobjective optimization, evolutionary multi-criterion opitimization," *Lect. Notes Comput. Sci.*, Vol. 1993, 126–140, 2001.

21. Chakravarty, S., R. Mittra, and N. B. Williams, "Application of a micro-genetic algorithms (MGA) to the design of broad-band microwave absorbers using multiple frequency selective surface screen buried in dielectrics," *IEEE Trans. Antennas Propag.*, Vol. 50, No. 3, 284–296, Mar. 2002.

22. Fallahi, A., M. Mishrikey, C. Hafner, and R. Vahldieck, "Efficient procedures for the optimization of frequency selective surfaces," *IEEE Trans. Antennas Propag.*, Vol. 56, No. 5, 1340–1349, May 2008.

23. Mori, T., R. Murakami, Y. Sato, F. Campelo, and H. Igarashi, "Shape optimization of wideband antennas for microwave energy harvesters using FDTD," *IEEE Trans. Magn.*, Vol. 51, No. 3, 8000804, Mar. 2015.

24. Tsuji, Y. and M. Koshiba, "A finite element beam propagation method for strongly guiding and longitudinally varying optical waveguides," *J. Lightwave Technol.*, Vol. 14, No. 2, 217–222, Feb. 1996.

25. Koshiba, M. and Y. Tsuji, "A wide-angle finite-element beam propagation method," *IEEE Photon. Technol. Lett.*, Vol. 8, No. 9, 1208–1210, Sept. 1996.

26. Yasui, T., M. Koshiba, and Y. Tsuji, "A wide-angle finite element beam propagation method with perfectly matched layers for nonlinear optical waveguides," *J. Lightwave Technol.*, Vol. 17, No. 10, 1909–1915, Oct. 1999.

27. Nolting, H.-P. and R. März, "Results of benchmark tests for different numerical BPM algorithms," *J. Lightwave Technol.*, Vol. 13, No. 2, 216–224, Feb. 1995.

28. Okamoto, K., *Fundamentals of Optical Waveguides*, 2nd edition, Academic Press, Burlington, MA, USA, 2005.